

# Journal of Astronomical Telescopes, Instruments, and Systems

AstronomicalTelescopes.SPIEDigitalLibrary.org

## Utilizing freeform optics in dynamic optical configuration designs

Isaac Trumper  
Daniel P. Marrone  
Dae Wook Kim

**SPIE.**

Isaac Trumper, Daniel P. Marrone, Dae Wook Kim, "Utilizing freeform optics in dynamic optical configuration designs," *J. Astron. Telesc. Instrum. Syst.* **5**(3), 035005 (2019), doi: 10.1117/1.JATIS.5.3.035005.

# Utilizing freeform optics in dynamic optical configuration designs

Isaac Trumper,<sup>a</sup> Daniel P. Marrone,<sup>b</sup> and Dae Wook Kim<sup>a,b,\*</sup>

<sup>a</sup>University of Arizona, James C. Wyant College of Optical Sciences, Tucson, Arizona, United States

<sup>b</sup>University of Arizona, Department of Astronomy, Tucson, Arizona, United States

**Abstract.** A linear field of view (FOV) K-mirror system used for image derotation is presented as a case example for how to leverage freeform surfaces in dynamic optical configuration design. As the K-mirror rotates about the optical axis, points in the FOV sample the surface at distinct locations, allowing for highly local control of the system aberrations. This methodology is distinct from the typical benefits associated with freeform surfaces, and as such broadens the uses of freeform optics into the category of systems that exhibit changing optical configurations. We show that compared to an on-axis or off-axis conic design, the freeform surface has better distortion correction abilities. Furthermore, a real pupil is generated by the K-mirror system and analyzed for uniformity. The design ideas presented for the K-mirror are discussed in the context of astronomical applications, where systems may benefit from these techniques. © 2019 Society of Photo-Optical Instrumentation Engineers (SPIE) [DOI: [10.1117/1.JATIS.5.3.035005](https://doi.org/10.1117/1.JATIS.5.3.035005)]

Keywords: freeform optics; K-mirror; instrument design.

Paper 19017 received Feb. 10, 2019; accepted for publication Jun. 24, 2019; published online Jul. 12, 2019.

## 1 Introduction

We present an alternative application of freeform optics in systems that change their optical configuration in a dynamic fashion. Typically, by including a freeform optical element in an optical system, the designer can achieve greater control over the optical behavior in the form of more optical power, greater FOV, and compactness. Although these benefits are typically gained when implementing freeform optical elements, the idea of considering the system configuration dynamics as a mode of leveraging the surface type is different. For this work, we take the example of a linear FOV K-mirror system with optical power used for image derotation. However, other cases of configuration dynamics (including those with two-dimensional FOVs) such as an off-axis zoom system are possible.

A K-mirror is widely used in astronomical optics, from the submillimeter<sup>1</sup> to the infrared,<sup>2</sup> where linear FOV systems are also common. We use this application space to illustrate the benefits and trade-offs of utilizing freeform optics in dynamic optical configurations. The principle behind applying freeform optical elements in a system with configuration dynamics is based on recognizing the variation in surface sampling with configuration, regardless of the other system parameters such as FOV, aperture, and wavelength. To demonstrate the use of freeform optical elements in such systems, we compare the K-mirror system performance with and without freeform surfaces. Optical performance metrics including imaging, distortion, and pupil illumination are contrasted and presented in the context of real-world considerations found in K-mirrors in astronomical instruments.

### 1.1 Freeform Optics

Freeform surfaces have changed the landscape of imaging optics,<sup>3</sup> which was made possible by advances in the fields

of design,<sup>4,5</sup> fabrication,<sup>6,7</sup> testing,<sup>8,9</sup> and alignment.<sup>10,11</sup> Freeforms can be employed to reduce system size, increase system FOV, or resolution compared to rotationally symmetric lenses and mirrors. Leveraging freeforms in an off-axis system allows the designer to more compactly package the design while maintaining the optical performance of an on-axis system. This is particularly important in reflective systems where on-axis systems are typically obscured or require a large packaging volume if using off-axis sections of a rotationally symmetric design. Furthermore, on-axis systems with a high-aspect ratio (linear fields of view) can also benefit from freeform optical surfaces.<sup>12</sup>

An alternative to the more general freeform surface is an off-axis aspheric surface,<sup>13–16</sup> which has more heritage in the optical fabrication and testing community.<sup>17–19</sup> An off-axis asphere may be able to give the designer sufficient degrees of freedom (DOF) to achieve the desired optical performance, while keeping the surface description less complex than that of a freeform surface. Aspheric surfaces have polynomial descriptions that are formulated to help improve manufacturability while retaining quick optimization convergence through their orthogonality. This is important when many terms in the polynomial description are used to achieve the desired optical performance. However, the fabrication and testing challenges of an off-axis asphere are similar to that of a freeform surface, dependent on the exact aspheric departure. Fabrication requires a local generating/polishing method, which requires specialized tooling. Off-axis sections produced on a diamond turning machine require more complex spindle setups, or tooling, to achieve the nonrotationally symmetric final surface. This same complexity in fabrication is found in the production of freeform surfaces. Many testing methods for aspheric surfaces require computer generated holograms (CGH), which can be fabricated to produce a null for practically any surface. This means that the cost of making a CGH for an off-axis aspheric surface is identical to that of the fully freeform surface type. Alternative testing methods for

\*Address all correspondence to Dae Wook Kim, E-mail: [letter2dwk@hotmail.com](mailto:letter2dwk@hotmail.com)

aspheric surfaces employ subaperture interferometric stitching, which is also used in the freeform domain, albeit with potentially more complex stitching techniques.

However, there are disadvantages of using a freeform optic, which are found in manufacturing, testing, and alignment. Computer numerically controlled machines are able to produce complex freeform shaped mirror surfaces with the required precision for millimeter-wavelength optics. This greatly reduces the complexity of fabricating a freeform compared to shorter wavelengths (visible or infrared), but care still needs to be taken to ensure that the right surface is produced. Furthermore, freeform surfaces generally require extra test and alignment features and datum surfaces, which can be machined into the same substrate concurrently with the optical surface in this scenario. The testing of a freeform is more difficult because the number of DOF that must be controlled increases. However, this complexity is mostly mitigated by using a laser tracker, since its absolute positioning accuracy is usually sufficient for the tolerances of a millimeter-wavelength optic. Given the difficulties briefly described above, the design must be carefully considered before applying freeform surfaces. Once the trade-offs are evaluated and a freeform surface is deemed necessary, then the performance benefits of such a surface may be leveraged as described throughout this manuscript.

## 1.2 Image Derotation

When a telescope is mounted in an altitude-azimuthal (alt-az) configuration, the image at the focal plane rotates about the optical axis as the telescope tracks sources across the sky. For some astronomical applications, it is critical to counteract this image motion by derotating the FOV. Examples of such cases include slit spectroscopy and pushbroom-type telescopes. In this work, we will focus on one particular aspect of tracking a source with an alt-az mount such that its orientation and location do not change in the instrument focal plane. To achieve this property, both the telescope mount axes and a third rotation about the optical axis must be driven continuously. This is known as image (or field) derotation<sup>20</sup> and is implemented in general by either rotating the focal plane or optical elements to compensate for the rotation of the source on the sky as it transits. Image derotation through focal plane motion is generally simpler from the optical

perspective, but more difficult from the mechanical, electrical, and systems views, and therefore, not typically chosen. More common is optical image derotation, which can be achieved through a parity change.<sup>21</sup> The input optical axis is not deviated from the output axis to prevent the beam from precessing about the rotation axis, which leads to a host of reflective and refractive design combinations to be used for image rotation. A few classic examples of refractive image rotators are the: Dove, Abbe, and Pechan, while a reflective version of the Abbe is called the K-mirror due to the orientation of the three mirrors.

## 2 Optical Design of Dynamic K-Mirror Systems

A K-mirror is selected for this work because of its applications in astronomy where refractive options are less common due to the materials and wavelength ranges. To derotate the field, a K-mirror rotates the incoming light by an angle  $2\theta$  for every  $\theta$  rotation about its axis. A diagram showing how the orientation of the incoming beam is rotated about the axis of propagation through the reversal of parity is given in Fig. 1.

The folding angle of the K-mirror  $\gamma$ , defined as the angle between the incident and reflected light from the second mirror, determines the axial compactness of the system while the distance between the input optical axis and the second mirror  $H$  determines the lateral compactness as shown in Fig. 2. Given an axial length  $L$  and lateral height  $H$  of the K-mirror, the folding angle  $\gamma$  and spacing  $R$  of the mirrors are given by

$$R = \sqrt{H^2 + \left(\frac{L}{2}\right)^2}, \quad (1)$$

$$\gamma = 2 \arctan\left(\frac{L}{2H}\right), \quad (2)$$

which determines the angle of incidence (and reflection) on the first mirror:

$$\beta = \frac{1}{4}(\gamma + \pi), \quad (3)$$

where  $\beta$  is in radians. A small folding angle results in an axially compact rotator. However, the lateral size grows in order to

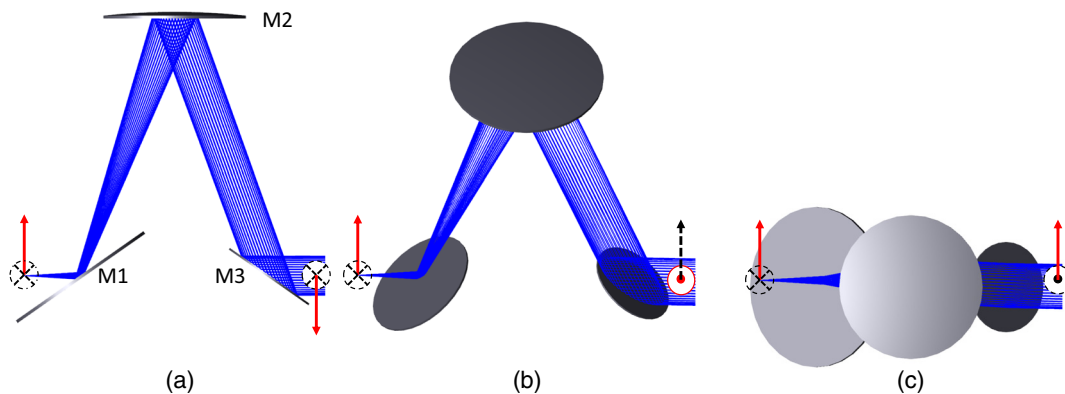


**Fig. 1** Schematic showing how the K-mirror system rotates the beam about the direction of propagation by twice the angle that the K-mirror is rotated. In (a) is the defined 0 deg angle of the K-mirror, with the system rotated by 45 deg in (b) and finally by 90 deg in (c). The same coordinate axes are given at the input to the K-mirror (dashed axis into the page, solid axis upward in the page), resulting in output coordinates that are rotated by twice the K-mirror rotation. M1, M2, and M3 are labels for the mirrors in system, where light travels from M1 to M2 and finally to M3.

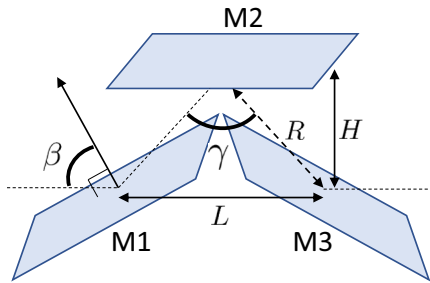


**Fig. 2** Diagram of the parameters used to define the layout of a K-mirror image rotator, where  $L$  and  $H$  could be specified by packing restrictions, which determine the required folding angle  $\gamma$ , spacing between mirrors  $R$ , and angle of incidence  $\beta$ . M1, M2, and M3 are the labels for the mirrors in the system, where light travels from M1 to M2 and finally to M3.

provide clearance between the first and last mirrors. Additional considerations arise when the image derotator is used in systems with off-axis fields, noncollimated spaces, or when polarization is a concern. When a field must pass through the K-mirror unvignetted, the spacing between the mirrors or folding angle needs to grow to compensate for the extra optical area used by the beam to prevent the mirrors from overlapping. Similarly, in a noncollimated space, the size of the mirrors must accommodate the changing beam diameters as they propagate and either diverge or converge depending on source location. Therefore, K-mirror systems are typically used in collimated spaces but with care can be applied to noncollimated optical spaces.

When using a K-mirror in a noncollimated space with off-axis fields, optically powered elements may be necessary in order to prevent the mirror sizes from growing unmanageably large.<sup>2</sup> Including optical power in the surfaces of the K-mirror achieves a more compact and versatile optical system because of the additional DOF.<sup>1</sup> However, the high angles of incidence of the input and output K-mirror reflections generate strong aberrations even for weakly powered surfaces.<sup>22</sup> Therefore, examples of powered K-mirrors in the literature confine optical

power to the second mirror (M2 in Fig. 2), which has the smallest angle of incidence. The shape of this second mirror is also usually a conic, either elliptical or parabolic,<sup>23</sup> with very weak optical power.

## 2.1 Dynamic Optical Configuration

Given that the second mirror in the K-mirror image derotator is an off-axis element, it will surely benefit from the application of freeform optics. Greater aberration control can be achieved with the freeform surface type compared to a conic, either on-axis or off-axis. Furthermore, as the K-mirror is rotated about its axis to perform image derotation, the location at which a field point samples the beam changes as a function of this angle. In this work, we present a view of utilizing the freeform surfaces given the dynamics of the K-mirror changing its optical configuration as a function of image derotation.

To highlight the capabilities of seeing an optical design in this manner, we will take a typical configuration of a K-mirror system placed immediately after a telescope focal plane, using the powered surface in the K-mirror to collimate the incoming light. A linear FOV is used in this setup, creating a line of image points on the telescope focal plane. As the K-mirror rotates, the beams move across the mirror surfaces, as shown in Fig. 3. This leads to the benefit of using a freeform surface instead of an off-axis conic or rotationally symmetric surface. With the freeform, one can attempt to correct the varying aberrations because the beams at the various angles sample different sections of the surface than before. An off-axis conic or rotationally symmetric surface does not have, or is limited in, this capability, and therefore, suffers from more significant aberrations.

Due to the location of the telescope focal plane with respect to the K-mirror system, the beams are more spatially separated on M1 than the other two mirrors, which, given the previous statements, may lead to the conclusion that M1 should be freeform. However, a better choice for the optical power is M2 due to the high angle of incidence on M1, which leads to increased manufacturing sensitivity. One may think of M1 as serving as a field corrector plate, where there is little to no overall optical power, but there is local correction. However, this role is

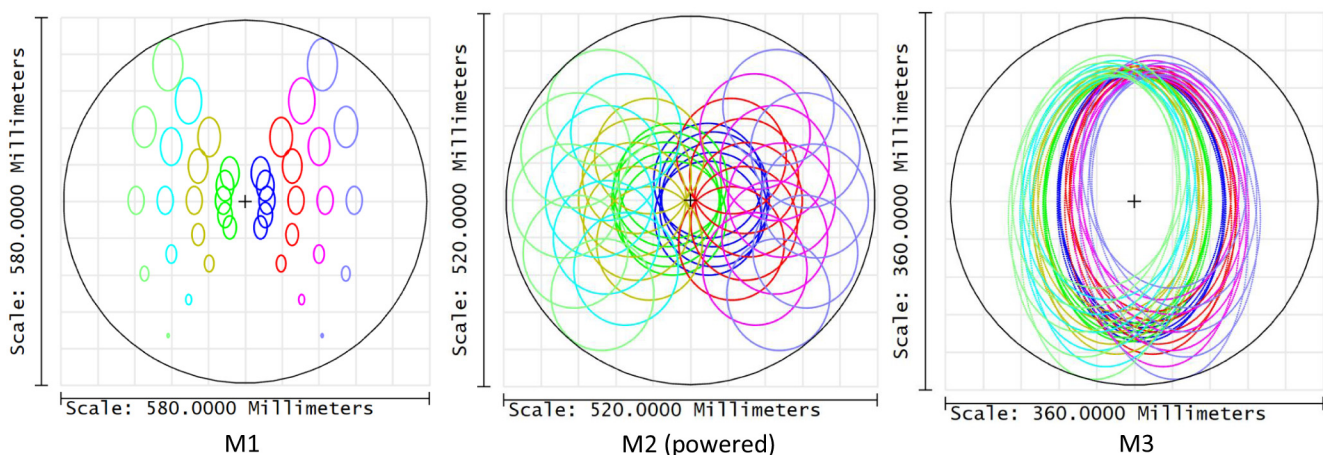


**Fig. 3** Beam footprints on the three K-mirror surfaces. Each color represents a point in the FOV, where the same colored footprints are from five separate K-mirror rotation angles ( $\theta = -45$  deg,  $-22.5$  deg,  $0$  deg,  $22.5$  deg, and  $45$  deg) showing how the beams sample the surfaces as a function of angle. The telescope focal plane is placed close to the center of the first K-mirror. The second surface in the K-mirror is a freeform, which was chosen because the angle of incidence is minimized, and therefore, the aberration contribution is reduced.

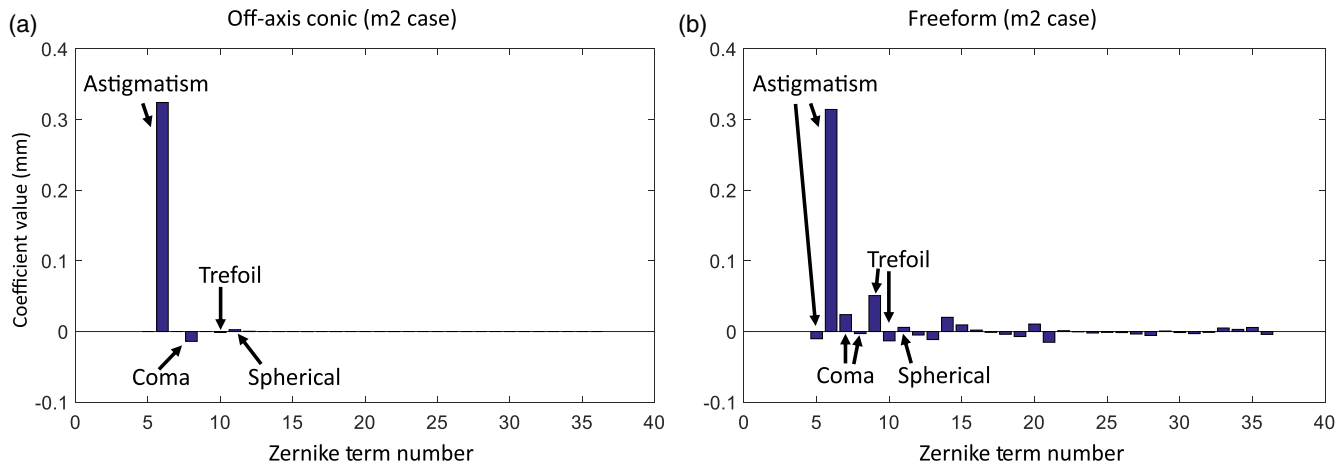


**Fig. 4** Surface decomposition of a powered surface in a K-mirror system whose surface profile is specified using (a) the off-axis conic parameters or (b) Zernike coefficients in standard ordering. The surface decomposition was performed with 36 Zernike terms in standard ordering over the circular aperture of the mirror.

complicated due to the sensitivity of output beam quality on small surface errors. Given these considerations, most designs will benefit from leaving M1 and M3 flat and allowing M2 to be a fully freeform surface.

### 2.1.1 Covariance of Zernike coefficients in off-axis conics

The parameters that define an off-axis conic surface are: radius of curvature, conic constant, off-axis distance, and aperture size. Shown in Fig. 4 are Zernike decompositions of an off-axis conic surface and a freeform surface in a K-mirror for the same optical configuration. A total of 36 Zernike terms in standard ordering were used to fit the surface data. Z4 (power) has been removed to improve visibility of the other terms. The off-axis conic and freeform surfaces have 3.76 and 3.764 mm of Z4, respectively. The amount of astigmatism in both surfaces is similar, but coma, trefoil, and higher terms are significantly different between the two since the off-axis conic terms have a defined covariance. We see that the off-axis conic has many fewer contributing Zernike terms than the freeform, leading to a lower flexibility in the type of aberration control that the surface can achieve. In terms of defining a surface in a dynamic optical configuration, such as a K-mirror, the reduced freedom of aberration control in the off-axis conic manifests itself in a lower optical performance. The freeform surface is able to generate the exact amount of each coefficient required to optimize the design performance while the off-axis conic has a fixed dependency between Zernike terms.

### 2.2 Freeform versus Off-Axis Conic versus On-Axis Conic

We will compare the optical performance obtained when using freeform versus an off-axis conic versus an on-axis conic as the surface type of the second mirror in a K-mirror system. Listed in Table 1 are the optical specifications for the simulation experiments, including the merit function parameters used to determine optical quality. The Strehl ratio and distortion specifications were chosen based on the diffraction limit and to minimize the distortion. Note that the object height parameter is the distance from the optical axis to the maximum extent of the object. The optical power in the K-mirror will be used to

**Table 1** Layout specifications defining the K-mirror test case. The object distance and entrance pupil locations are given with respect to the first K-mirror (M1 in Fig 5). These parameters were chosen to mimic a 12-m radio astronomy telescope on Kitt peak.<sup>24</sup>

Specification	Requirement
Object distance (mm)	-200
Object height (mm)	171.43
Entrance pupil dia. (mm)	12,000
Entrance pupil loc. (mm)	-96,200
Angle of incidence $\beta$ (deg)	55
Mirror spacing $R$ (mm)	1000
Folding angle $\gamma$ (deg)	40
Wavelength (mm)	1.0
Strehl ratio	>0.8
Distortion	Min.

collimate the beam, which will be analyzed using an image quality metric by placing an aberration-free paraxial lens after the K-mirror system to refocus the beam. Shown in Fig. 5 is the optical layout used for comparing the performance of the three design types. Another paraxial lens is used to create the real object plane by focusing collimated light such that the aperture stop of the system is placed on the first paraxial lens. This lens is not shown in Fig. 5 since it is much farther away and larger than the K-mirror system. This design format mimics the Kitt Peak 12 meter radio astronomy telescope geometry,<sup>24</sup> where the Cassegrain telescope serves the role of the first paraxial lens and the aft-optics replaces the second lens. The first paraxial lens has a focal length of 9600 mm and the second lens has a focal length of 1200 mm. The second lens in combination with the K-mirror instrument forms a 1-to-1 imaging system, resulting in an  $f$ -number ( $F/\#$ ) of 8. Continuing with the example of the radio

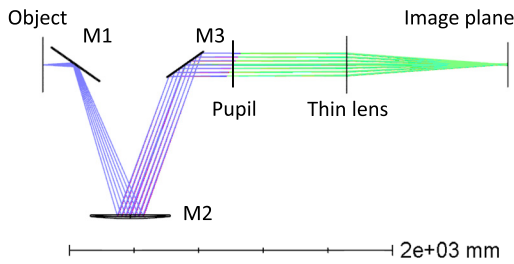


**Fig. 5** Optical layout of the K-mirror system used to perform the design comparison experiments. Note that this is one configuration of the K-mirror, where to produce the image derotation, the system (M1 to M3) rotates about the optical axis (horizontal), causing the light from the various fields to move on the optical surfaces.

astronomy telescope on Kitt Peak, we use a wavelength of 1 mm.

Using the same merit function to optimize all three designs, on-axis conic, off-axis conic, and freeform, we obtain the surface specifications given in Table 2. We see a similar base radius of curvature in both the freeform and off-axis conic surfaces, while the on-axis conic differs significantly because it cannot compensate for the off-axis configuration. However, the freeform surface is able to compensate for the configuration-dependent aberrations while the off-axis conic cannot. The freeform surface was specified using 36 terms of Zernike polynomials in

standard ordering. The coefficients for each polynomial and their corresponding Zernike coefficient are given in Table 3.

To highlight the local surface tailoring that the freeform system achieves, Fig. 6 shows the sag of M2 (panel a), with Zernike power (Z4) removed from the surface in panel (b). The dominant underlying surface shape in both surfaces is astigmatism to compensate for the off-axis imaging configuration, but the freeform surface has additional subaperture variations to correct the aberrations across the FOV and the rotation of the K-mirror. The changing and localized sampling of the M2 surface due to the dynamic configuration of the system allow the freeform surface to be used in a different manner. Shown in Fig. 7 are three discrete subapertures of the powered mirror seen by the beams in three different configurations of the K-mirror rotation. We have removed Zernike terms through astigmatism (Z1 to Z6) to highlight the local control that is gained using the freeform surface. Further, the residual coma (Z7 and Z8) in the off-axis conic that is not present in the freeform design shows the undesired covariance of the Zernike coefficients for that surface type specification. The optical aberration control mandates a local surface change, which is achievable using the freeform but not with the off-axis conic.

### 3 Optical Performance

Both optical designs surpass the Strehl ratio requirement, with a maximum root-mean-square focused spot radius of 2 mm. Note

**Table 2** Optimized optical specifications for M2. The freeform surface is also specified with Zernike polynomials in standard ordering whose coefficients are given in Table 3.

Design	Radius of curvature (mm)	Conic					
On-axis conic	2365	0.4106					
	Radius of curvature (mm)	Conic	Off-axis distance (mm)		Aperture size (mm)		
Off-axis conic	2723	0.1917	2106		500		
	Radius of curvature (mm)	Conic	X dec. (mm)	Y dec. (mm)	Z dec. (mm)	X tilt (deg)	Y tilt (deg)
Freeform	2400	17.48	115.63	62.913	3.502	1.582	-1.994

**Table 3** Coefficients of the freeform surface used in the K-mirror. The coefficients correspond to the first 36 Zernike polynomials in standard ordering, where Z1 to Z4 are not shown because they are all zero. Note that a normalization radius of 368.7 mm is used so the coefficients are unitless.

Term	Coefficient	Term	Coefficient	Term	Coefficient	Term	Coefficient
Z5	-1.459	Z6	-2.402	Z7	0.334	Z8	-1.879
Z9	-2.124	Z10	-0.419	Z11	-0.63	Z12	-1.391
Z13	-0.595	Z14	1.236	Z15	-0.381	Z16	-0.492
Z17	0.159	Z18	-0.162	Z19	-0.572	Z20	0.574
Z21	0.786	Z22	-0.061	Z23	-0.062	Z24	-0.246
Z25	-0.021	Z26	0.204	Z27	0.489	Z28	-0.078
Z29	0.03	Z30	-0.035	Z31	-0.044	Z32	-0.019
Z33	0.076	Z34	0.047	Z35	0.088	Z36	-0.062

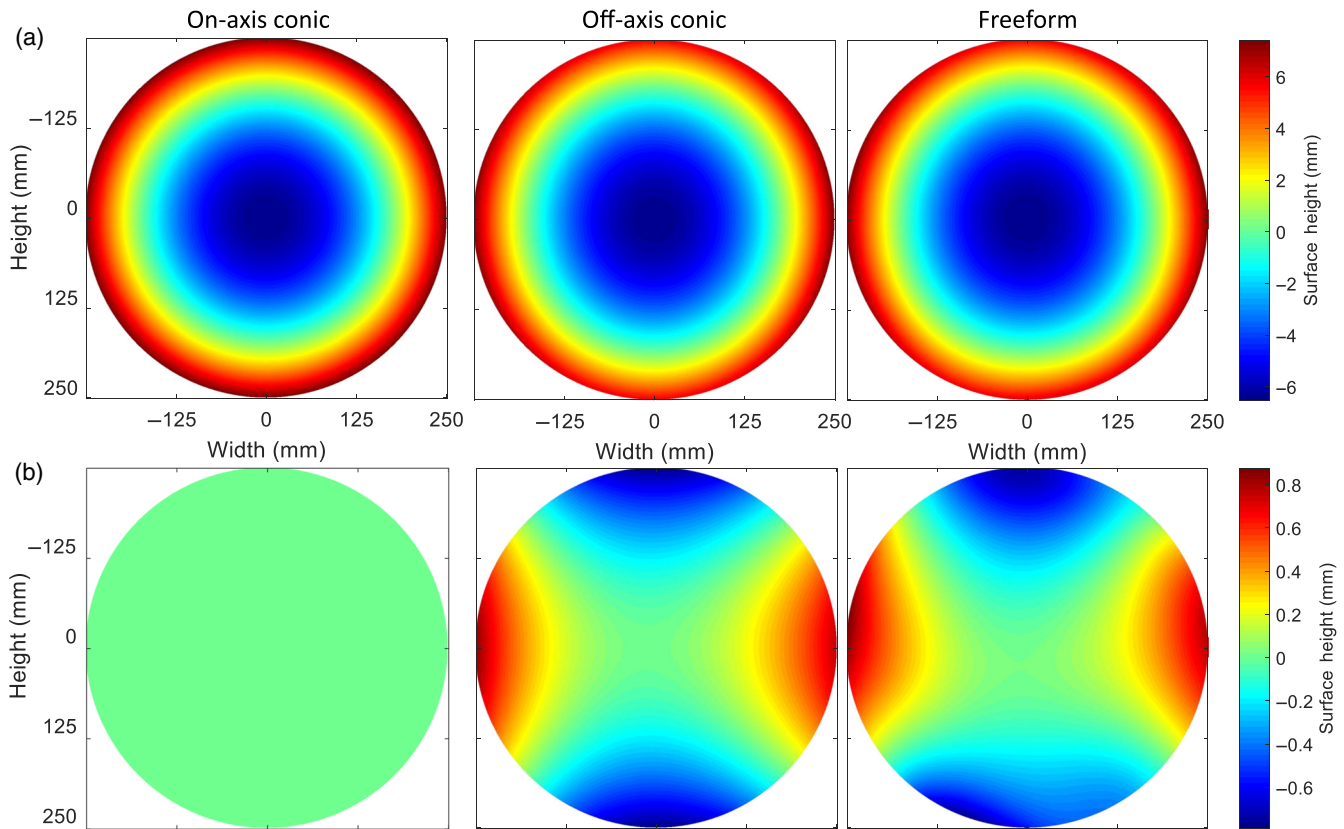


**Fig. 6** Surface sag maps of M2 in the K-mirror systems. (a) The full surface sag and (b) the Zernike power term (Z4) removed to highlight the local surface control achieved by using a freeform surface specification. The local control gained in the freeform surface means that configuration-dependent aberrations can be better corrected.

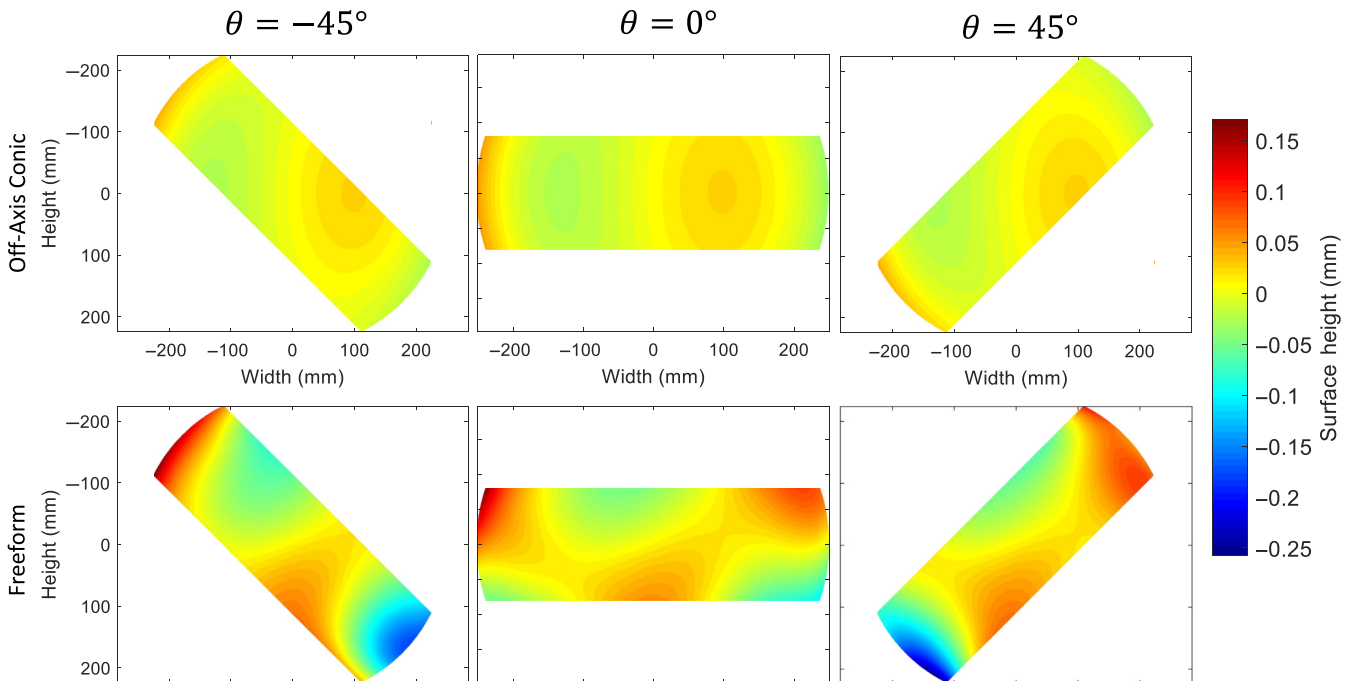


**Fig. 7** Subaperture samples of the powered mirror (as shown in Fig 6) in the K-mirror instrument, where each configuration is a rotation of the K-mirror about its axis by 45 deg. The freeform surface is able to generate the local surface control that the design requires while the off-axis conic is stuck with an entangled ratio of terms that are generated by obtaining the correct amount of astigmatism.

that at the system F/# of 8 and wavelength of 1 mm, the diffraction limited spot radius is 9.76 mm. The focusing requirements at this wavelength are not the driving factors in this design, rather minimizing the distortion is the most difficult aspect.

### 3.1 Distortion

The distortion in the system changes significantly between the two designs, where the freeform surface is able to achieve less distortion than the off-axis conic. Shown in Fig. 8 is the image plane for each design, with the focused spot from each configuration of the K-mirror superimposed on top of one another. Ideal focus positions are computed from a thin lens perspective given that the K-mirror and second paraxial lens form a 1-to-1 imaging system. Any variation in these focus locations with respect to the centroid of the focus is classified as a distortion and is characterized by computing the shift in location along the  $x$  and  $y$  coordinate axes. The values reported in Fig. 9 are the errors in the focus location for eight points in the FOV, averaged across the rotation of the K-mirror. The amount of distortion in field 6 is similar between all designs and is likely due to the nature of balancing the performance across many merit function operands. Also note that even though the average % distortion is lower for some fields in the on-axis conic case, the variation in position with K-mirror configuration is much worse as seen in Fig. 8. The freeform surface is able to tailor the optical performance with more finesse than the off-axis conic because we achieve local control over the surface for each position of the K-mirror. The configuration-dependent optimization utilizes a freeform surface in a new manner compared to prior work since the subaperture illuminated in each configuration is dynamically varying.

### 3.2 Lyot Stop Uniformity

Instruments that employ bolometers limited in sensitivity by thermal emission from their surroundings, such as those found in millimeter-wave astronomy, require low levels of stray-light since any unwanted light hitting the detectors is a source of unwanted photon noise that masks the weak signals of interest. To control this behavior, a pupil with a well-defined aperture is usually required. This is known as a Lyot stop,<sup>25</sup> which is

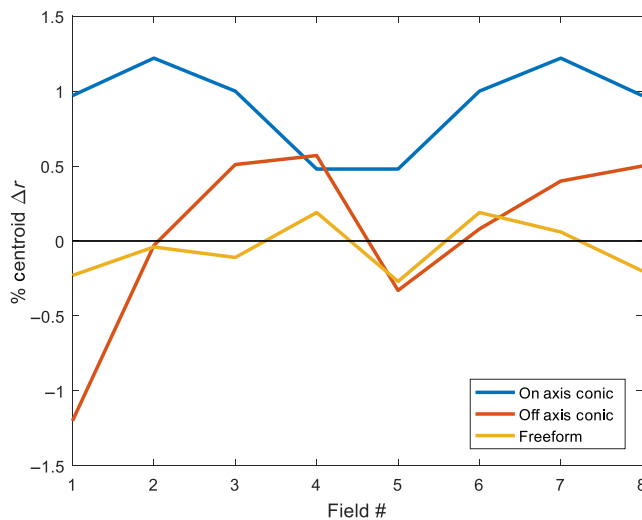


**Fig. 9** Percent radial difference in centroid location between the ideal and the as-designed coordinates for eight field points in the instrument FOV averaged across the 5 K-mirror configurations ( $\theta = -45$  deg,  $-22.5$  deg,  $0$  deg,  $22.5$  deg, and  $45$  deg).

typically placed within a cryogenic environment.<sup>26-28</sup> When utilizing a freeform surface in an instrument to achieve the required imaging and distortion performance, we must also take care to manage the Lyot stop uniformity. Unfortunately, the control that allows a freeform surface to perform so well in tailoring its imaging performance is the same freedom that can degrade and limit the quality of the Lyot stop. Examining the pupil generated by the design that was optimized for imaging performance presented in Fig. 8 and specified in Table 2, we notice that the freeform has a worse quality Lyot stop compared to the off-axis conic. Plotting the rays from the edge of the entrance pupil for each field point and multiple positions of the K-mirror, we obtain the beam footprint diagrams shown in Fig. 10. The on-axis conic has the worst pupil because the astigmatism is uncorrected and it cannot form a uniform pupil. However, the local variations (low-to-mid spatial frequencies) of the freeform surface create higher-order deviations from a circle, which also vary more strongly with K-mirror angle that are not present in

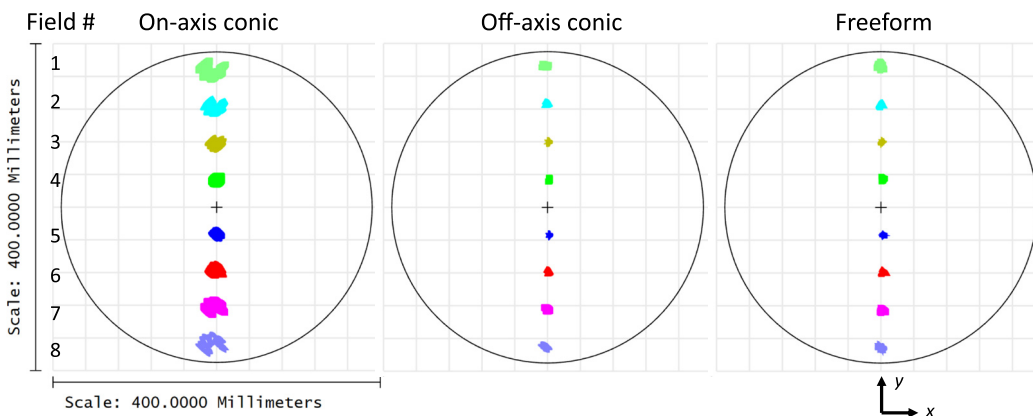


**Fig. 8** Comparison between the distortion correction achieved between the on-axis conic, off-axis conic, and freeform designs. The image planes for each design are shown with the focused spots from each K-mirror position on top of one another. Distortion is defined as the shift in focus location with respect to the ideal focus, computed using a thin lens model. The distortion of each point in the FOV is computed in all three designs, as given in Fig. 9.

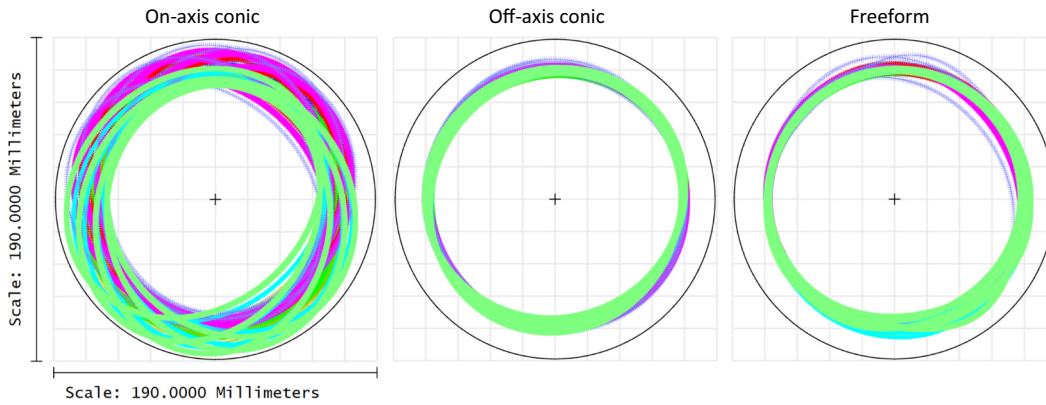


**Fig. 10** Footprint diagrams of the pupil created by the K-mirror system for the three surface types used in the powered optical element (M2). The off-axis conic generated the most uniform and symmetric pupil due to the lower local variance compared to the freeform design. A footprint diagram is generated by tracing and recording the location of rays from the outside edge of the entrance pupil.

**Table 4** Best fit standard errors of the ellipse radii for the pupil in the K-mirror instrument shown in Fig 10.

Best fit ellipse	On-axis conic	Off-axis conic	Freeform
X radius (%)	7.7	0.58	0.84
Y radius (%)	7.1	1.6	3.4

the off-axis conic. These effects can be seen in the purple rays in the freeform pupil, where the different K-mirror positions do not correlate as well and the localized deviations from the overall circular shape.

If we fit the ray positions from each configuration of the K-mirror (across the entire FOV) with an ellipse, the resulting standard errors in the ellipse radii are given in Table 4. From the fitted data, we see the same result in the pictorial representation such that the off-axis conic has a more centered and circular pupil with less variation compared to the freeform or on-axis conic. The off-axis conic has the least variation because it does not induce mid-spatial variations like the freeform, which can lead to a slightly more anamorphic pupil, but it can still account for the off-axis configuration, unlike the on-axis conic. These data highlight the need to take extra care when working with freeform optical surfaces. Furthermore, working with pupils in a freeform design is difficult because the variation across the aperture of the optical surfaces creates nonuniformities in the pupil that are hard to balance with the desired variations in the image plane.

### 3.3 Design Considerations

Not all K-mirror designs should utilize freeform or powered surfaces. The instrument design must warrant their application or else the design becomes unnecessarily complicated. The points raised in the discussion in Sec. 1.1 should be carefully considered when looking at the trade-offs between these surface types.

## 4 Conclusion

We presented a unique use of freeform optics to correct for configuration-dependent aberrations by obtaining local control of the surface. One such application is in image derotation when

a K-mirror system is used with optical power. For the scenario of image derotation, the freeform system was able to achieve lower distortion without sacrificing imaging performance but comes at the cost of a slightly less uniform pupil. A real, accessible pupil is sometimes necessary in situations where image derotation is also employed, such as radio astronomy. Therefore, a minor trade-off between imaging/distortion and pupil uniformity exists when employing a freeform surface in the K-mirror for image derotation. We provided a few considerations on the optimization process and the design space opened by freeform optics when performing image derotation using a K-mirror with optical power and a linear FOV. By comparing three different surface types (on-axis conic, off-axis conic, and  $xy$ -polynomial freeform), we provide a reference point for which optical performance is available given these different design options.

### Acknowledgments

The authors would like to thank Zemax for the student license of OpticStudio, which made this research project possible. They would also like to thank the Technology Research Initiative Fund (TRIF) Optics/Imaging Program, through the College of Optical Sciences at the University of Arizona, the postprocessing of Freeform Optics project supported by the Korea Basic Science Institute, the II-VI Foundation Block-Gift Program, and the Friends of Tucson Optics (FoTO) Endowed Scholarships in Optical Sciences. The authors also acknowledge support from the National Science Foundation through Award No. AST-1653228. Disclosures: The authors have no relevant financial interests in the manuscript and no other potential conflicts of interest to disclose.

### References

- W. S. Holland et al., "SCUBA: a common-user submillimetre camera operating on the James Clerk Maxwell telescope," *Mon. Not. R. Astron. Soc.* **303**(4), 659–672 (1999).
- I. S. McLean et al., "Design and development of NIRSPEC: a near-infrared echelle spectrograph for the Keck II telescope," *Proc. SPIE* **3354**, 566–578 (1998).
- K. P. Thompson and J. P. Rolland, "Freeform optical surfaces: a revolution in imaging optical design," *Opt. Photonics News* **23**(6), 30–35 (2012).
- K. Garrard et al., "Design tools for freeform optics," *Proc. SPIE* **5874**, 58740A (2005).

5. G. W. Forbes, "Characterizing the shape of freeform optics," *Opt. Express* **20**, 2483–2499 (2012).
6. F. Fang et al., "Manufacturing and measurement of freeform optics," *CIRP Ann.* **62**(2), 823–846 (2013).
7. T. Blalock, K. Medicus, and J. D. Nelson, "Fabrication of freeform optics," *Proc. SPIE* **9575**, 95750H (2015).
8. E. Savio, L. D. Chiffre, and R. Schmitt, "Metrology of freeform shaped parts," *CIRP Ann.* **56**(2), 810–835 (2007).
9. P. Su et al., "Aspheric and freeform surfaces metrology with software configurable optical test system: a computerized reverse Hartmann test," *Opt. Eng.* **53**, 031305 (2013).
10. K. Fuerschbach et al., "Assembly of a freeform off-axis optical system employing three  $\varphi$ -polynomial Zernike mirrors," *Opt. Lett.* **39**, 2896–2899 (2014).
11. M. Beier et al., "Development, fabrication, and testing of an anamorphic imaging snap-together freeform telescope," *Appl. Opt.* **54**, 3530–3542 (2015).
12. F. Duerr, Y. Meuret, and H. Thienpont, "Potential benefits of free-form optics in on-axis imaging applications with high aspect ratio," *Opt. Express* **21**, 31072–31081 (2013).
13. L. Mertz, "Geometrical design for aspheric reflecting systems," *Appl. Opt.* **18**, 4182–4186 (1979).
14. S. A. Lerner and J. M. Sasian, "Optical design with parametrically defined aspheric surfaces," *Appl. Opt.* **39**, 5205–5213 (2000).
15. H. Chase, "Optical design with rotationally symmetric NURBS," *Proc. SPIE* **4832**, 10–24 (2002).
16. R. N. Youngworth and E. I. Betensky, "Lens design with Forbes aspheres," *Opt. Syst. Des.* **7100**, 71000W (2008).
17. L. N. Allen, J. J. Hannon, and R. W. Wambach Jr., "Final surface error correction of an off-axis aspheric petal by ion figuring," *Active Adapt. Opt. Compon.* **1543**, 190–200 (1992).
18. H. P. Stahl, "Aspheric surface testing techniques," in *Fabrication and Testing of Aspheres*, Vol. 24, Optical Society of America, p. T2 (1999).
19. J. H. Burge et al., "Fabrication and testing of 1.4-m convex off-axis aspheric optical surfaces," *Proc. SPIE* **7426**, 74260L (2009).
20. P. T. Wallace, "A rigorous algorithm for telescope pointing," *Proc. SPIE* **4848**, 125–136 (2002).
21. D. Swift, "Image rotation devices—a comparative survey," *Opt. Laser Technol.* **4**(4), 175–188 (1972).
22. K.-F. Schuster et al., "The IRAM 230-GHz multibeam SIS receiver," *Proc. SPIE* **4015**, 260–267 (2000).
23. K.-F. Schuster et al., "A 230 GHz heterodyne receiver array for the IRAM 30 m telescope," *Astron. Astrophys.* **423**(3), 1171–1177 (2004).
24. Arizona Radio Observatory, "Arizona Radio Observatory equipment summary and status 12M Telescope," <https://aas.org/files/resources/arostatus28july2017.pdf> (accessed 03 July 2019).
25. B. Lyot, "The study of the solar corona and prominences without eclipses (George Darwin lecture, 1939)," *Mon. Not. R. Astron. Soc.* **99**, 580–594 (1939).
26. J. R. Eimer et al., "The cosmology large angular scale surveyor (CLASS): 40 GHz optical design," *Proc. SPIE* **8452**, 845220 (2012).
27. J. W. Fowler et al., "Optical design of the Atacama Cosmology Telescope and the millimeter bolometric array camera," *Appl. Opt.* **46**, 3444–3454 (2007).
28. J. Glenn et al., "Bolocam: a millimeter-wave bolometric camera," *Proc. SPIE* **3357**, 326–334 (1998).

**Isaac Trumper** received his BS degree in optics from the Institute of Optics at the University of Rochester in 2015. He is a PhD graduate from the Large Optics Fabrication and Testing Group of the College of Optical Sciences at the University of Arizona. He founded and is currently working at an optical consulting company, Intuitive Optical Design Lab. His current research interests include optical metrology, optical design, and optical software development.

**Daniel P. Marrone** is an associate professor of astronomy at the University of Arizona. His research combines observational techniques and innovative instruments to study fundamental physics, cosmology, and galaxy formation. He has been developing millimeter-wavelength instruments for 20 years for ground-based and balloon-borne applications.

**Dae Wook Kim** is an assistant professor of optical sciences and astronomy at the University of Arizona. He has been working in the optical engineering field for more than 10 years, mainly focusing on very large astronomical optics such as the 25-m diameter Giant Magellan Telescope primary mirrors. His main research area covers the precision freeform optics fabrication and various metrology topics such as interferometric test systems using computer generated holograms, direct curvature measurements, and dynamic deflectometry systems. He is currently a chair/co-chair of the Optical Manufacturing and Testing conference (SPIE) and the Optical Fabrication and Testing conference (OSA). He is a senior member of OSA and SPIE and has been serving as an associate editor for the journal *Optics Express*.